Available online at www.sciencedirect.com
SCIENCE DIRECT
Journal of Power Sources 154 (2006) 232–238
JOURNAL OF POWER SOURCES
www.elsevier.com/locate/jpowsour

Developments of high-voltage all-solid-state thin-film lithium ion batteries

J. Schwenzel, V. Thangadurai, W. Weppner *

Chair for Sensors and Solid State Ionics, Faculty of Engineering, University of Kiel, Kaiserstrasse 2, D-24143 Kiel, Germany

Received 27 January 2005; accepted 14 March 2005
Available online 13 June 2005

Abstract

Powders of $Li_2MMn_3O_8$ (M = Fe, Co) were prepared by glycine nitrate combustion from the corresponding metal nitrates. The reaction products were pressed into pellets with the addition of 20 wt.% excess $LiNO_3$, which were used as targets for e-beam evaporation. A high-voltage all-solid-state thin-film lithium ion battery was demonstrated by the sequential deposition of spinel structured $Li_2MMn_3O_8$ (M = Co, Fe) as positive electrode by e-beam evaporation, LiPON as electrolyte, and metallic Al as negative electrode by sputtering in N_2 and Ar gas mixtures with specific power and gas flow rates. A lithium ion conductivity of $\sim 10^{-6}$ S cm^{-1} was observed for the optimized thin-film LiPON electrolyte prepared under the condition of a chamber pressure of 2.6×10^{-2} mbar and a power of 60–100 W. The chemical diffusion coefficient ($\tilde{D}$) was found to be in the range 10^{-13} to 10^{-12} cm^2 s^{-1} for any composition x of $Li_{2-x}MMn_3O_8$ (M = Fe, Co) in the range from 0.1 to 1.6 by employing the galvanostatic intermittent titration technique (GITT). AC impedance studies revealed a charge transfer resistance of 260–290 Ω, a double layer capacity of ∼45–70 μF for an electrode area of 6.7 cm^2.

Keywords: Chemical diffusion coefficient; All-solid-state batteries; Li-ion batteries

1. Introduction

At present, there is a strong interest to develop materials for all-solid-state high-voltage lithium or lithium-ion secondary batteries due to their potential superior properties compared to conventional liquid/gel based batteries [1]. All-solid-state lithium batteries are leak proof, exhibit high safety performance, are mechanically robust and may be used over a wide range of temperature. Solid-state inorganic electrolytes have high decomposition voltages up to about 6 V against lithium metal and may be, accordingly, employed together with high-voltage lithium cathode materials. For example, lithium oxynitrides $Li_{3-x}PO_{4-y}N_y$ (LiPON) [2] and garnet-like structure $Li_6BaLa_2Ta_2O_{12}$ [3] exhibit high ionic conductivity and high electrochemical stability at room temperature.

In general, solid lithium electrolytes have a transference number of the lithium ions of 1. This is in contrast to common liquid and polymeric electrolytes, where both cations and anions are mobile. Often, transference numbers of the lithium ions are much smaller than those of the anions [4–6]. This high mobility of other ions than lithium may lead more readily to the formation of solid electrolyte interfacial (SEI) layers, which may cause deterioration and limit the life-time of the batteries. The negligible mobility of ions other than the electroactive ones in the solid state may provide a superior chemical stability. Depending on the lithium activity, however, electronic species may become important at high and low lithium activities.

Solid lithium-ion electrolytes have in general a lower Li^+-ion conductance than liquid/gel electrolytes. However, the application of thin-film technology offers a solution to this problem. For example, physical vapour deposition (PVD) methods that include sputtering, electron beam evaporation (EBE) and ablation may be used to prepare thin-film nano- to

* Corresponding author. Tel.: +49 431 880 6201; fax: +49 431 880 6203.
E-mail address: ww@tf.uni-kiel.de (W. Weppner).

0378-7753/$ – see front matter © 2005 Elsevier B.V. All rights reserved.
doi:10.1016/j.jpowsour.2005.03.223

micro-sized metal and metal oxide layers. The thin-films show lower resistance compared to those of much thicker samples. Therefore, the low electrical conductivity of solid electrolytes will not be a problem for their application in galvanic cells. Furthermore, besides thin-film electrolytes, thin-film electrodes are advantageous because of lower diffusion lengths (faster equilibration) compared to thick films. This allows the development of all-solid-state batteries, especially lithium system, which show high power densities besides high energy densities. It should be also mentioned that all-solid-state batteries will have low gravimetric energy density due to the low weight of the active materials compared to conventional rocking-chair batteries.

Current all-solid-state thin-film Li-battery developments make use of LiC_6, elemental lithium or inorganic compounds such as silicon–tin oxynitrides, Sn_3N_4, Zn_3N_2 or metal films including Cu and In as anodes, $LiCoO_2$ and $LiMn_2O_4$ as cathodes and LiPON as electrolyte. The preparation of Li thin-films requires special evaporation equipment and the prepared films may not be exposed to air. In order to overcome this technical problem, we replaced the Li anode by Al metal, which forms alloys with Li by electrochemical reaction [7]. We have also replaced the conventional $LiCoO_2$ cathode with other alternative high-voltage cathode materials, e.g., 3D spinel structured $Li_2MMn_3O_8$ (M = Fe, Co) [8], to increase the operating voltage.

The $Li_2MMn_3O_8$ (M = Fe, Co) electrode shows two reversible plateaus during the charging and discharging cycle at 4 V/Li and 5.3 V/Li [8]. The former plateau is due to the valence change from Mn^{3+} to Mn^{4+} (4 V) (reaction (1)) and the latter one is due to the M^{3+} to M^{4+} oxidation process (5.3 V) (reaction (2)) according to the electrochemical deintercalation/intercalation reactions:

$$Li_2M^{III}Mn^{III}Mn_2^{IV}O_8 \underset{\text{discharge}}{\overset{\text{charge}}{\rightleftarrows}} Li_{2-x}M^{III}Mn_{1-x}^{III}Mn_x^{IV}Mn_2^{IV}O_8 + xLi^+ + xe^- \quad (1)$$

$$Li_{2-x}M^{III}Mn_{1-x}^{III}Mn_x^{IV}Mn_2^{IV}O_8 \underset{\text{discharge}}{\overset{\text{charge}}{\rightleftarrows}} Li_{2-(x+y)}M_{1-y}^{III}M_y^{IV}Mn_{1-x}^{III}Mn_x^{IV}Mn_2^{IV}O_8 + (x+y)Li^+ + (x+y)e^- \quad (2)$$

The theoretical energy density of the 4 V region is 290 Wh kg^{-1} ($x = 1$) and of the 5 V region 370 Wh kg^{-1} ($y = 1$). For both together, i.e., $x + y = 2$, the value of $Li_2CoMn_3O_8$ is 660 Wh kg^{-1} [8]. In comparison, the theoretical energy density of $Li_{1-x}CoO_2$ for the 3.9 V plateau and $x = 0.5$ is 534 Wh kg^{-1}. We show in the present work that all-solid-state thin-film high-voltage batteries are feasible by employing metallic Al as anode and spinel structured $Li_2MMn_3O_8$ (M = Fe, Co) as cathode and LiPON as electrolyte. The chemical diffusion coefficient of the cathode materials was determined by the galvanostatic intermittent titration technique (GITT) [9–11] and from AC impedance data [12].

2. Experimental aspects

2.1. Preparation of LiPON solid electrolyte thin-films

LiPON thin-film electrolytes were prepared by reactive rf-sputtering (Alcatel, model-450, Annecy, France) using a commercially available Li_3PO_4 target in N_2 gas with the optimized conditions of a chamber pressure of 2.6×10^{-2} mbar and applying a power of 60–100 W. Table 1 lists the various employed sputtering conditions.

2.2. Preparation of aluminium metal thin-films

Aluminium metal thin-films were deposited onto an alumina substrate by rf-sputtering using Al metal target. Pure Ar gas was purged with a flow rate of 20 sccm, maintaining a constant pressure of 1×10^{-2} mbar in the sputtering chamber. Applying a power of 150 W resulted in a sputtering rate of about 35 nm min^{-1}.

2.3. Preparation of thin-film cathodes

Thin-film $Li_2MMn_3O_8$ (M = Fe, Co) was prepared by e-beam evaporation using an PLS-500 electron beam evaporation equipment from Pfeiffer Vacuum, Asslar, Germany. The powders for the targets were prepared by glycine nitrate combustion. High purity lithium nitrate [$LiNO_3$], cobalt nitrate [$Co(NO_3)_3{\cdot}6H_2O$], iron nitrate [$Fe(NO_3)_3{\cdot}9H_2O$], manganese nitrate [$Mn(NO_3)_2{\cdot}4H_2O$] and glycine [H_2NCH_2COOH] (∼1 mol of glycine per 2 mol of nitrates) were mixed in the required molar ratio and dissolved in a minimum amount of de-ionized water. The solutions were heated to 300 °C using a heating plate. After complete evaporation of water, sudden ignition has occurred and resulted in black coloured powders. The powders were collected and annealed at 700 °C for 2 h in air using alumina crucibles. The powders were pressed into pellets by

Table 1
Geometrical parameters and electrical properties of the LiPON thin-film electrolyte

Target/substrate (cm)	Sputtering power (W)	Contact area (cm^2)	Thickness (μm)	R (Ω)	σ_{RT} (S cm^{-1})	C_{geom} (nF)	ε
7	60	0.04	0.65	1000	1.7×10^{-6}	1.4	27
5	100	1	0.88	85	1.0×10^{-6}	25	23
7	100	7.84	0.90	10	1.4×10^{-6}	127	20

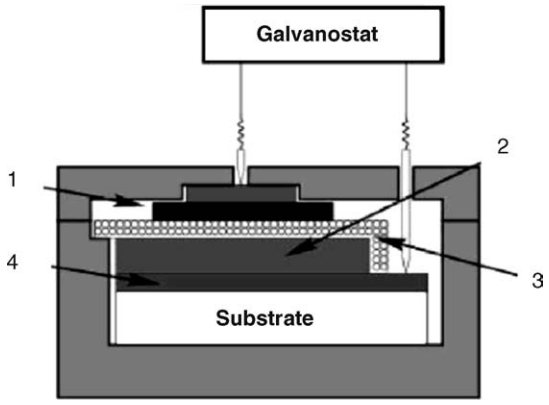

Fig. 1. Experimental set-up for the characterization of the individual thin-film electrode and electrolyte films using auxiliary liquid electrolytes (1) Li, (2) electrode film (500–1000 nm), (3) microporous flat sheet membrane electrolyte ($LiPF_6$ in EC:DEC) and (4) Pt 10% Rh (100 nm).

isostatic pressure using an excess of 20 wt.% $LiNO_3$.These targets employed for the e-beam evaporation. Without addition of excess $LiNO_3$, we see an Mn_2O_3 impurity phase in the films. After evaporation, the thin-films were annealed in air at 700 °C for 2 h with heating and cooling rates of 1 °C min^{-1}. The sample powders and thin-films were characterized structurally by Powder X-ray Diffraction (XRD) (SEIFERT 3000 powder X-ray diffractometer, Cu Kα, Ahrensburg, Germany). For XRD analysis, thick films were deposited onto Si-wafers.

2.4. Electrochemical characterization

Fig. 1 shows a schematic representation of the experimental set-up used for the individual characterization of electrode thin-films. For the liquid electrochemical characterization, the Al films were covered with a microporous flat sheet membrane with a soaked-in liquid electrolyte of 1 mol l^{-1} $LiPF_6$ in EC:DEC (2:1) solution from Merck. These two parts were pressed together within a stainless steel container with the addition of a piece of lithium (Aldrich, 99.9%) on top as a reference electrode. The electrochemical performance of the electrode materials was studied by constant current discharge and coulometric titration employing a liquid electrolyte (1 mol l^{-1} $LiPF_6$ in EC:DEC (2:1)) versus lithium. The first two cycles were run under a continuous constant current density of 10 μA cm^{-2}. The third cycle was a coulometric titration by applying a sequence of current density of 10 μA cm^{-2} for specific time intervals, and reading the open circuit voltage in-between after equilibration.

2.5. All-solid-state lithium ion cell preparation

The galvanic cells

$$Al|LiPON|Li_2MMn_3O_8 \quad (M = Co, Fe) \qquad (1)$$

were deposited onto alumina substrates with a typical LiPON thickness of 1 μm. Sputtered Pt 10 wt.% Rh films were used as current collectors. The various layers were prepared according to the sequence: (i) sputtering of the Pt/Rh current collector layer, (ii) e-beam evaporation of one of the cathode materials ($Li_2MMn_3O_8$ (M = Co, Fe)) (∼500 nm), (iii) annealing at 700 °C in air, (iv) rf-sputtering of the LiPON layer (∼1 μm) and (v) rf-sputtering of the aluminium layer (100 nm). All electrochemical measurements were made inside a glove box under purified argon gas atmosphere. AC Impedance measurements were performed by using an HP 4192 A Impedance and Gain Phase Analyzer (5 Hz–13 MHz) to determine the conductivity and the dielectric constant of the electrolyte as a function of temperature. The galvanic cells were discharged/charged galvanostatically under a constant current of 5 μA, and coulometric titrations were performed with a current of 10 μA at an electrode area of 6.7 cm^2 at room temperature.

3. Results and discussion

3.1. Ionic conductivity of thin-film LiPON solid electrolyte

Fig. 2 shows the typical complex impedance diagram for a thin-film LiPON electrolyte of 800 nm in thickness in the temperature range between 26 and 60 °C. A single semicircle at the high frequency side and a tail at the low frequency side were observed, which is a typical behaviour for lithium ion blocking electrodes [13]. Semicircles and characteristic capacitive impedances were observed, which increase with decreasing frequencies. The resistance (R) and the geometric capacity (C_{geom}) for different geometrical set-ups and the calculated dielectric constant ε are compiled in Table 1 together with the sputtering conditions.

The Arrhenius plots of the lithium ion conductivity for LiPON thin-films prepared at different sputtering conditions (Table 1) and geometrical parameters are given in Fig. 3. The ionic conductivity of about 10^{-6} S cm^{-1} is obtained at room

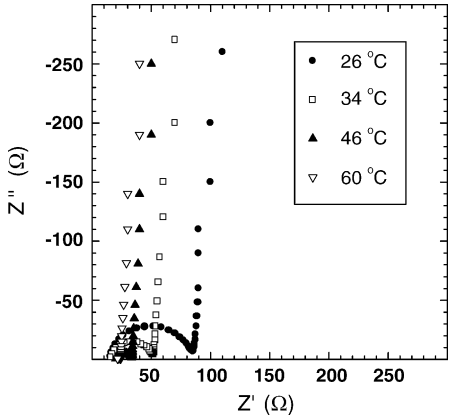

Fig. 2. AC impedance plots of LiPON at a few temperatures measured in the frequency range 5 Hz–13 MHz using lithium ion blocking electrodes. Electrode area A = 1 cm^2, and thickness of the LiPON electrolyte d = 800 nm.

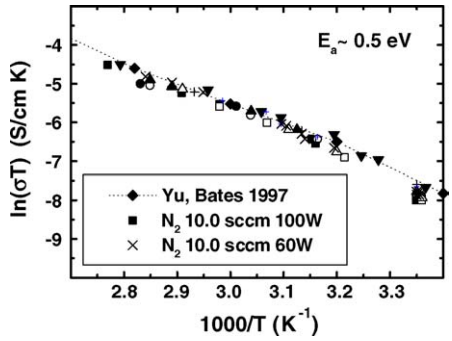

Fig. 3. Arrhenius plot for several samples of sputtered LiPON-films sandwiched between Pt 10 wt.% Rh strips. The different data points correspond to different samples with different areas (0.04–6.7 cm^2) and thicknesses (1–1.5 μm) sputtered with an applied power of 100 W. (×) sample sputtered with an applied power of 60 W. Literature data of LiPON are shown by the broken line [2].

temperature with an activation energy of about 0.5 eV. These values are comparable to those reported in the literature [2].

3.2. Al negative electrode thin-films

The system lithium–aluminium has a wide solid solution α region at room temperature [7]. The LiAl alloy shows a voltage in the regime 300 mV against metallic Li at ∼400 °C. The chemical diffusion coefficient of LiAl has a quite high value of 2.4×10^{-6} cm^2 s^{-1} at 415 °C [10,14]. The extrapolated value at room temperature is in the range of 10^{-10} to 10^{-9} cm^2 s^{-1}, which is in agreement with literature values. The electrochemical behaviour of the Al thin-films is shown in Fig. 4. The first two cycles were galvanostatic (constant currents) runs without interruption, which were followed by coulometric titration with a current density of 10 μA cm^{-2}. It is clearly observed that the α–β two-phase regime has a voltage between 300 and 400 mV versus elemental Li at room temperature.

3.3. High-voltage cathodes and all-solid-state lithium batteries

XRD patterns of the $Li_2CoMn_3O_8$ powder were taken directly after preparation and after annealing at 700 °C as

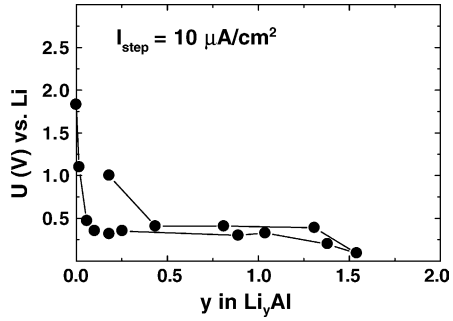

Fig. 4. Third coulometric titration cycle of a sputtered Al thin-film.

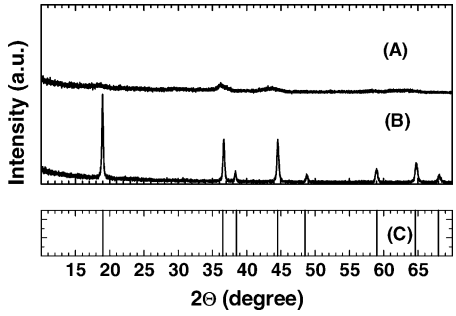

Fig. 5. Powder XRD-pattern of the $Li_2CoMn_3O_8$ powder (A) directly after preparation and (B) after annealing in air at 700 °C for 2 h. The X-ray pattern is in agreement with the data of JCPDS Card No. 48:261 (C).

shown in Fig. 5. The as-prepared powder is X-ray amorphous. After annealing in air at 700 °C for 1 h it becomes crystalline and shows the diffraction lines corresponding to spinel lattice (Table 2). The X-ray pattern is in agreement with the data of the JCPDS file (No. 48:261) for this compound. Similar data were obtained for the corresponding Fe member, $Li_2FeMn_3O_8$. Fig. 6 shows the X-ray pattern of the evaporated $Li_2CoMn_3O_8$ thin-films. By adding an excess of 20 wt.% $LiNO_3$ to the powder mixture before evaporation and by feeding 20 cm^3 min^{-1} O_2 gas into the chamber during evaporation, and providing at the same time a constant pressure of about 10^{-5} mbar, the patterns of the films agree best with those of the JCPDS Card No. 48:261 for $Li_2CoMn_3O_8$. Without providing the oxygen to the evaporation chamber

Table 2
Powder XRD data of $Li_2MMn_3O_8$ (M = Fe, Co) prepared by glycine nitrate combustion method

h	*k*	*l*	$Li_2FeMn_3O_8$			$Li_2CoMn_3O_8$		
			$d_{obs.}$ (Å)	$d_{cal.}$ (Å)	$I_{obs.}$	$d_{obs.}$ (Å)	$d_{cal.}$ (Å)	$I_{obs.}$
1	1	1	4.733	4.747	100	4.678	4.695	100
3	1	1	2.475	2.479	54	2.450	2.451	50
2	2	2	2.371	2.373	14	2.344	2.347	13
4	0	0	2.054	2.055	65	2.031	2.033	48
3	3	1	1.886	1.886	12	1.866	1.865	8
3	3	3	1.583	1.582	24	1.565	1.565	16
4	4	0	1.454	1.453	40	1.438	1.437	21
5	3	1	1.392	1.389	15	1.374	1.374	8
			a = 8.222(3) (Å)			a = 8.132(2) (Å)		

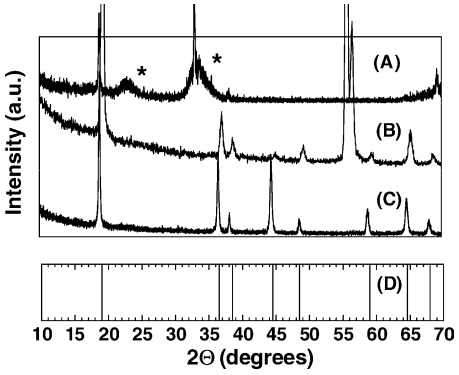

Fig. 6. X-ray pattern of $Li_2CoMn_3O_8$ thin-films (A) thin-film evaporated without additional $LiNO_3$ and O_2 gas, i.e., the Mn_2O_3 phase (*) was found, (B) thin-film evaporated with additional 20 wt.% $LiNO_3$ in the powder mixture. For comparison the powder X-ray data of $Li_2CoMn_3O_4$ after annealing at 700 °C for 2 h in air are shown (C). JCPDS Card No. 48.261.

and the additional $LiNO_3$, the Mn_2O_3 phase was found in addition in the XRD pattern (Fig. 6).

The solid-state galvanic cell

$$\text{Al|LiPON|Li}_2\text{CoMn}_3\text{O}_8\text{|Pt 10 wt.\% Rh} \quad (2)$$

was characterized electrochemically by galvanostatic charge and discharge measurements using constant currents. The results are shown in Fig. 7 for a current of 5 μA for an electrode area of 6.7 cm^2. The first cycle consisted of a charging process until a voltage of 4.8 V was reached, whereas a maximum voltage of 5 V was allowed during the following cycles. There exist two plateaus which are expected from the valence changes of Mn at 3.7 V versus Al, LiAl and of Co at around 4.8 V versus Al, LiAl.

3.4. Chemical diffusion coefficients of lithium in the $Li_2MMn_3O_8$ (M = Fe, Co) cathodes

The coulometric titration curve of the galvanic cell (2) is shown in Fig. 8. The hysteresis is due to the lack of complete thermodynamic equilibria in-between the individual steps. The chemical diffusion coefficient ($\tilde{D}$) could be obtained with the short-term titration curves using the relationship [9–11,14]:

$$\tilde{D} = \frac{4}{\pi}\left(\frac{IV_M}{zFA}\right)^2\left[\left(\frac{dE}{d\delta}\right)/\left(\frac{dE_t}{d\sqrt{t}}\right)\right]^2, \quad t \ll \frac{L^2}{\tilde{D}} \quad (3)$$

where I, L, V_M, z, F, δ and A represent the electrical current, thickness, molar volume of the electrode, Faraday's constants, stoichiometric change and cross-sectional area common to both the electrolyte and the sample electrode, respectively. The value of $dE/d\delta$ is directly obtained from the slope of the coulometric titration curve, which is obtained by plotting the steady-state equilibrium voltage of the electrode against the composition or the stoichiometric parameter after each galvanostatic titration step. The value of $dE/d\sqrt{t}$ is determined from the measurement of

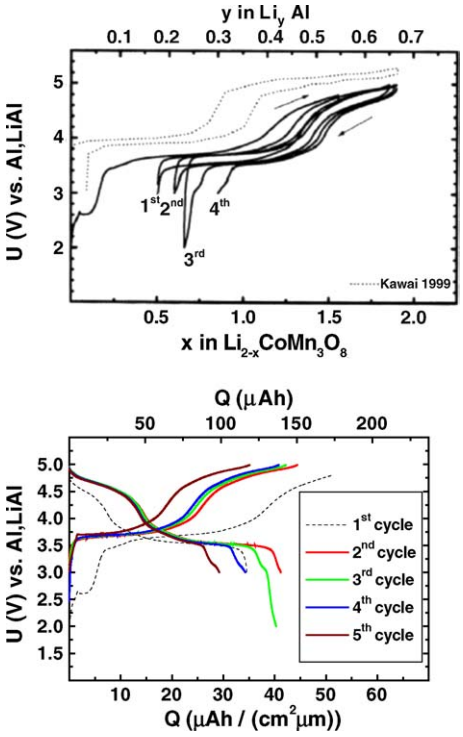

Fig. 7. (A and B) Galvanostatic charge and discharge measurements of the complete solid state cell set-up, i.e., Al |LiPON| $Li_2CoMn_3O_8$| Pt 10 wt.% Rh, using a constant current of 5 μA and an electrode area of 6.7 cm^2. The thickness of $Li_2CoMn_3O_8$, LiPON and Al layers is 500 nm, 1 μm and 100 nm, respectively. During the first cycle, the cell was charged until a voltage of 4.8 V was reached whereas a maximum voltage of 5 V was allowed during the following cycles.

voltage as a function of time during the constant current pulse.

The chemical diffusion coefficient may be also determined from the long time relaxation behaviour, when a linear variation of the cell voltage with time should be observed. If the slope is sufficiently constant, the diffusion coefficient is derived from the difference of the intersection of the straight line in the voltage versus time plot with the voltage axis at

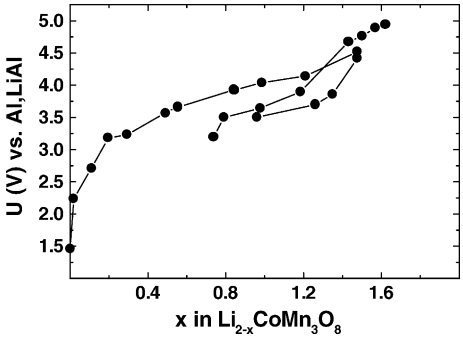

Fig. 8. Coulometric titration curve of the cell set-up Al |LiPON| $Li_2CoMn_3O_8$| Pt 10 wt.% Rh. Non-equilibrium data points were taken to achieve faster information on the system. The applied current was 5 μA and the electrode area was 6.7 cm^2.

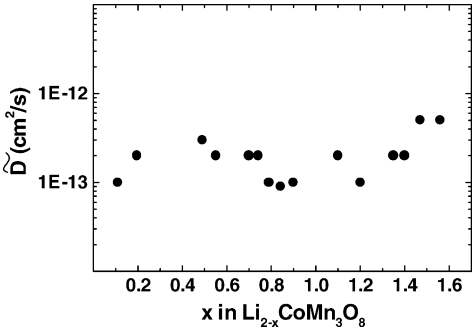

Fig. 9. Chemical diffusion coefficients ($\tilde{D}$) as calculated from the voltage transients of the single steps. The chemical diffusion coefficient scatters in a range between 10^{-13} and 10^{-12} cm^2 s^{-1} for the composition x from 0.1 to 1.6 in $Li_{2-x}CoMn_3O_8$.

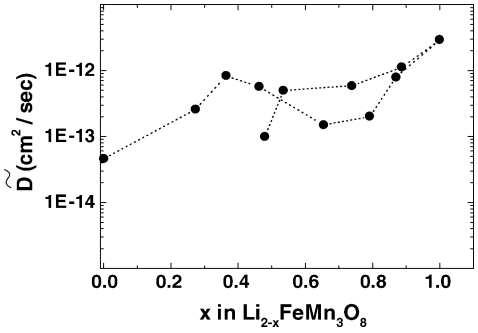

Fig. 11. Chemical diffusion coefficient ($\tilde{D}$) as calculated from the voltage transients of the single steps. The chemical diffusion coefficient scatters in a range between 10^{-13} and 10^{-12} cm^2 s^{-1} for the composition x from 0 to 1 in $Li_{2-x}FeMn_3O_8$.

$t = 0$ when the current was initiated and the initial voltage observed immediately after switching on the constant electrical current. The difference of these two voltages is expressed as E_Δ. The relationship is given by [9]:

$$\tilde{D} = \frac{ILV_M}{3E_\Delta zFA}\left(\frac{\partial E}{\partial \delta}\right), \quad t > \frac{L^2}{\tilde{D}} \tag{4}$$

and permits the determination of $\tilde{D}$ over the compositional change involved in the titration pulse. Results of the chemical diffusion coefficient being calculated from the voltage transients of the sequence of single steps are shown in Fig. 9. The chemical diffusion coefficient is in the range between 10^{-13} and 10^{-12} cm^2 s^{-1} for the composition x from 0.1 to 1.6 in $Li_{2-x}CoMn_3O_8$. Figs. 10 and 11 show the electrochemical characterization of the corresponding Fe-containing electrode $Li_{2-x}FeMn_3O_8$. The chemical diffusion coefficient of the LiAl negative electrode is about three orders of magnitude higher than that of the positive electrode materials. Accordingly, we believe that the diffusion of Li into and out of the cathode is the rate determinating process [15]. The diffusion coefficient values are about three orders of magnitude lower compared to those of $Li(M_{1/6}Mn_{11/6})O_4$ (M = Mn, Co, (Co, Al)) [16].

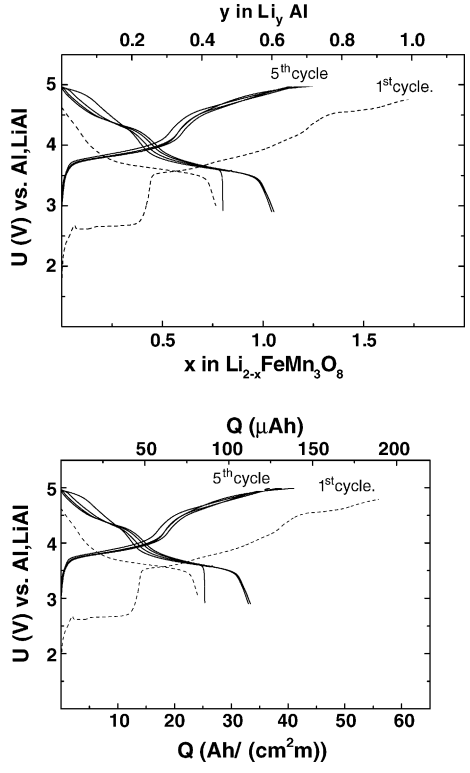

Fig. 10. Galvanostatic charge and discharge measurements of the cell set-up Al |LiPON| $Li_2FeMn_3O_8$| Pt 10 wt.% Rh. The applied current was 5 μA and the electrode area was 6.7 cm^2.

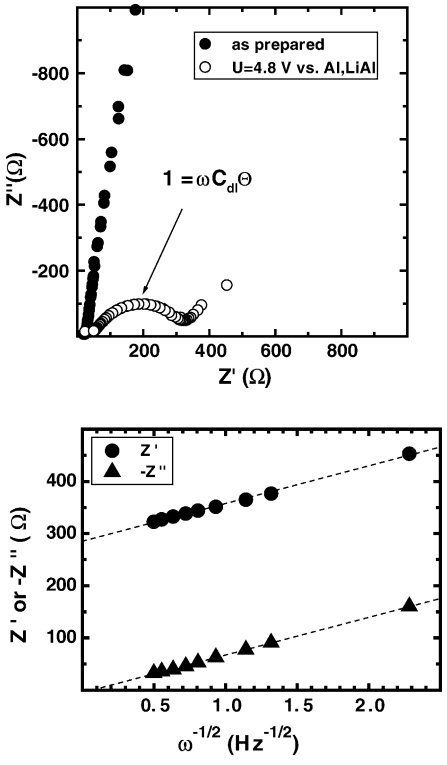

Fig. 12. Impedance plot of Al |LiPON| $Li_2CoMn_3O_8$| Pt 10 wt.% Rh for the as-prepared state and in the charged state of ~4.8 V vs. Al, LiAl.

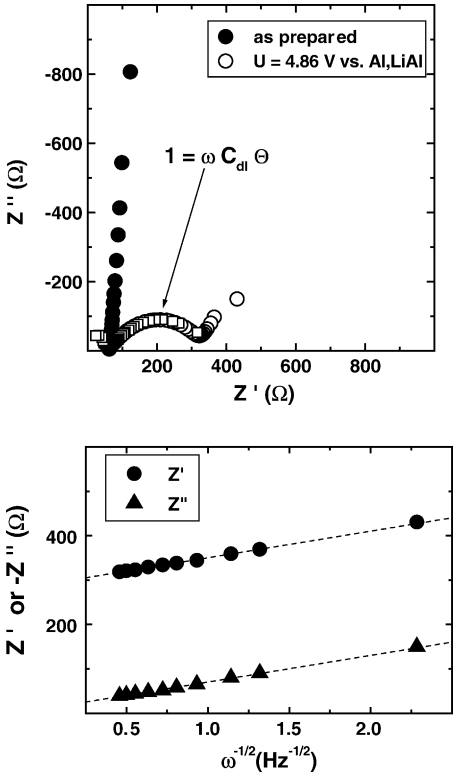

Fig. 13. Impedance plot of Al |LiPON| $Li_2FeMn_3O_8$| Pt 10 wt.% Rh for the as-prepared state and in the charged state of ∼4.8 V vs. Al, LiAl.

The results of impedance measurements performed directly after preparation and in the charged state at around 4.8 V versus Al, LiAl are shown in Figs. 12 and 13. For the as-prepared galvanic cells, the impedance diagram shows a behaviour similar to that obtained for blocking electrodes. There is a tail at low frequencies, and a single semicircle appears at higher frequencies. In the charged state, the impedance data changed largely in the lower frequency regime. The values for the charge transfer resistance (Θ) and double layer capacity (C_{dl}) calculated from these impedance measurements are 290 Ω and 45 μF, respectively. The chemical diffusion coefficient was calculated using the AC impedance data by the method of Ho et al. [12]. Diffusion coefficient values in the order of 10^{-12} cm^2 s^{-1} were obtained, which is consistent with GITT-method values.

We see that the capacity of the galvanic cell decreases with further cycling. This may be due to the following factors: (i) low kinetics of the positive electrode, (ii) high charge transfer resistance, (iii) poor electrode–electrolyte contact due to slight volume expansion of the negative electrode and (iii) formation of unwanted reaction products at the electrode–electrolyte interfaces. Accordingly, further work is required to improve the cycle behaviour of the presently investigated high-voltage lithium secondary batteries.

4. Conclusions

All-solid-state thin-film batteries are feasible by employing an Al anode and LiPON electrolyte fabricated by subsequent deposition of these materials by sputtering. High-voltage cathode electrode powders of $Li_2MMn_3O_8$ (M = Fe, Co) were prepared by employing the glycine combustion method. The thin-films of electrodes were obtained by electron beam evaporation with the addition of 20 wt.% $LiNO_3$ to the powder sample and under an oxygen partial pressure of 10^{-5} mbar during the evaporation process. These thin-film cells could be operated between 3 and 5 V versus Al, LiAl. The chemical diffusion coefficients for these materials, as determined by the galvanostatic intermittent titration technique, resulted in values for both materials in the range of 10^{-13} to 10^{-12} cm^2 s^{-1}.

References

[1] (a) C. Julien, G.A. Nazri, Solid State Batteries: Materials Design and Optimization, Kluwer Academic Publishers, Boston, 1994;
(b) J.B. Bates, N.J. Dudney, B. Neudecker, A. Ueda, C.D. Evans, Solid State Ionics 135 (2000) 33–45.
[2] X. Yu, J.B. Bates, G.E. Jellison Jr., F.X. Hart, J. Electrochem. Soc. 144 (1997) 524–532.
[3] (a) V. Thangadurai, W. Weppner, Adv. Funct. Mater. 15 (2005) 107–112;
(b) V. Thangadurai, W. Weppner, J. Power Sources 142 (2005) 339–344.
[4] T.B. Reddy, S. Hossain, in: D. Linden, T.B. Reddy (Eds.), Handbook of Batteries, third ed., McGraw-Hill, New York, 2002, pp. 34.1–34.62 (Chapter 34).
[5] F. Croce, B. Appetecchi, L. Persi, B. Scrosati, Nature 394 (1998) 456–458.
[6] P.G. Bruce, F.M. Gray, in: P.G. Bruce (Ed.), Solid State Electrochemistry, Cambridge University Press, Cambridge, 1995, pp. 119–162.
[7] W.C. Maskell, J.R. Owen, J. Electrochem. Soc. 132 (1985) 1602–1607.
[8] H. Kawai, M. Nagata, H. Tukamoto, A.R. West, J. Power Sources 81–82 (1999) 67–72.
[9] W. Weppner, R.A. Huggins, J. Electrochem. Soc. 124 (1977) 1569–1578.
[10] C.J. Wen, B.A. Boukamp, R.A. Huggins, W. Weppner, J. Electrochem. Soc. 126 (1979) 2258–2266.
[11] W. Weppner, R.A. Huggins, Z. Phys. Chem. 108 (1977) 105–122.
[12] C. Ho, I.D. Raistrick, R.A. Huggins, J. Electrochem. Soc. 127 (1980) 343–350.
[13] V. Thangadurai, R.A. Huggins, W. Weppner, J. Power Sources 108 (2002) 64–69.
[14] W. Weppner, R.A. Huggins, J. Electrochem. Soc. 125 (1978) 7–14.
[15] J. Schwenzel, V. Thangadurai, W. Weppner, New trends in intercalation compounds for energy storage and conversion, in: K. Zaghib, C.M. Julien, J. Prakash (Eds.), ECS Proceedings, PV2003-20, 2003, pp. 573–583.
[16] K.M. Shaju, G.V. Subba Rao, B.V.R. Chowdari, J. Mater. Chem. 13 (2003) 106–113.